Quantitative Measurement of Nanoparticle Halo Formation around Colloidal Microspheres in Binary Mixtures

Fan Zhang, Gabrielle G. Long,* Pete R. Jemian, and Jan Ilavsky

Advanced Photon Source, Argonne National Laboratory, Argonne, Illinois 60439

Valeria T. Milam† and Jennifer A. Lewis

Frederick Seitz Materials Research Laboratory, Materials Science and Engineering Department, University of Illinois at Urbana−Champaign, Urbana, Illinois 61801

Received October 4, 2007. Revised Manuscript Received March 19, 2008

A new colloidal stabilization mechanism, known as nanoparticle "haloing" (Tohver, V.; Smay, J. E.; Braem, A.; Braun, P. V.; Lewis, J. A. *Proc. Natl. Acad. Sci. U.S.A.* **2001**, *98*, (16), 8950−8954), has been predicted theoretically and inferred experimentally in microsphere−nanoparticle mixtures that possess high charge and size asymmetry. The term "halo" implies the existence of a nonzero separation distance between the highly charged nanoparticles and the negligibly charged microspheres that they surround. By means of ultrasmall-angle X-ray scattering, we have quantified the microsphere−nanoparticle separation distance as well as the number of nanoparticles and their lateral separation distance within the self-organized halos that form in these binary mixtures.

Introduction

Colloidal suspensions[1] enjoy widespread use in applications ranging from food science[2] to advanced materials,[3,4] for example, drug carriers,[5,6] photonic crystals,[4,7,8] ceramics, [9]and coatings.[10] In most systems of practical importance, van der Waals forces must be balanced by Coulombic, steric, or other repulsive interactions to provide control over suspension stability. Nanoparticle engineering is a new paradigm by which these interactions may be regulated.[11] We recently demonstrated that binary mixtures possessing high size and charge asymmetry, in which microspheres are negligibly charged and nanoparticles are highly charged, experience a rich phase behavior that transitions from a colloidal gel to a stable fluid and subsequently to a colloidal gel with increasing nanoparticle concentration.[11,12] We attributed the stabilizing transition to nanoparticle "haloing" around the microspheres, which serves to mitigate their van der Waals attraction.[11,12] System stability is ultimately reversed at higher nanoparticle concentrations, where flocculation ensues. This dynamic haloing effect has been predicted by recent theoretical[13] and numerical studies[14−16] and shown to be enhanced by a weak colloid−nanoparticle attraction. Yet, the exact origin and structure of the nanoparticle halos that form around each colloidal microsphere is still debated.

This novel stabilization route has been observed experimentally in binary mixtures composed of silica microspheres and zirconia nanoparticles,[11] silica microspheres and polystyrene nanoparticles,[16,17] and silica sol and alumina nanoparticles.[18] Nanoparticle haloing has been inferred by measuring the effective microsphere zeta potential induced by the presence of highly charged nanoparticles, quantifying the extent of nanoparticle adsorption onto the microsphere surfaces, and direct imaging of these mixtures by confocal laser scanning microscopy. However, due to the large size difference (∼100-fold) between the microspheres and nanoparticles, resolving the spatial distribution of nanoparticles around the microspheres is difficult.

In this paper, we report ultrasmall-angle X-ray scattering (USAXS) measurements of the structure of silica microsphere−zirconia nanoparticle mixtures that quantify the extent of nanoparticle halo formation in this system. This technique offers the distinct advantage of covering four decades of q range ($10^{-4} \sim 1$ Å^{-1}), where $q = (4\pi/\lambda)\sin(\theta)$, λ is the X-ray wavelength, and 2θ is the angle of scattering; hence, it covers a size range that encompasses both the microspheres and nanoparticles and is well suited for quantitative investigation of this system. We begin by introducing the binary mixtures used in the experiments and the experimental setup. The description and analysis of the USAXS data follow. Finally, we discuss our results and how our observations further the understanding of this novel stabilization mechanism.

Experimental Methods

Material System. Binary mixtures are prepared from uniform silica microspheres (Geltech; Alachua, FL) with an average radius

† Current address: School of Materials Science and Engineering, Georgia Institute of Technology, 771 Ferst Drive, N.W., Atlanta, Georgia 30332-0245.

(1) Russel, W. B.; Saville, D. A.; Schowalter, W. A. *Colloidal Dispersions*. Cambridge University Press: New York, 1992.
(2) Dickinson, E. *Colloids Surf.* **1989**, *42*, 191–204.
(3) Lewis, J. A. *Curr. Opin. Solid State Mater. Sci.* **2002**, *6*, 245–250.
(4) Xia, Y. N.; Gates, B.; Yin, Y. D.; Lu, Y. *Adv. Mater.* **2000**, *12*, 693–713.
(5) Caruso, F. *Adv. Mater.* **2001**, *13*, 11–22.
(6) Hagan, S. A.; Coombes, A. G. A.; Garnett, M. C.; Dunn, S. E.; Davis, M. C.; Illum, L.; Davis, S. S.; Harding, S. E.; Purkiss, S.; Gellert, P. R. *Langmuir* **1996**, *12*, 2153–2161.
(7) Lee, W.; Chan, A.; Bevan, M. A.; Lewis, J. A.; Braun, P. V. *Langmuir* **2004**, *20*, 5262–5270.
(8) Zhang, Z. L.; Keys, A. S.; Chen, T.; Glotzer, S. C. *Langmuir* **2005**, *21*, 11547–11551.
(9) Lewis, J. A. *J. Am. Ceram. Soc.* **2000**, *83*, 2341–2359.
(10) Sumida, T.; Wada, Y.; Kitamura, T.; Yanagida, S. *Langmuir* **2002**, *18*, 3886–3894.
(11) Tohver, V.; Smay, J. E.; Braem, A.; Braun, P. V.; Lewis, J. A. *Proc. Natl. Acad. Sci. U.S.A.* **2001**, *98*, 8950–8954.
(12) Tohver, V.; Chan, A.; Sakurada, O.; Lewis, J. A. *Langmuir* **2001**, *17*, 8414–8421.
(13) Karanikas, S.; Louis, A. A. *Phys. Rev. Lett.* **2004**, *93*, 248303.
(14) Liu, J.; Luijten, E. *Phys. Rev. E* **2005**, *72*, 061401.
(15) Liu, J. W.; Luijten, E. *Phys. Rev. Lett.* **2004**, *93*, 247802.
(16) Barr, S. A.; Luijten, E. *Langmuir* **2006**, *22*, 7152–7155.
(17) Chan, A. T.; Lewis, J. A. *Langmuir* **2005**, *21*, 8576–8579.
(18) Kong, D. Y.; Yang, H.; Yang, Y.; Wei, S.; Wang, H. B.; Cheng, B. J. *Mater. Lett.* **2004**, *58*, 3503–3508.

10.1021/la702968n CCC: $40.75 © XXXX American Chemical Society
Published on Web 05/29/2008

of 0.285 ± 0.01 μm and a density of 2.25 g/cm^3 and hydrous zirconia nanoparticles (Zr 10/20; Nyacol Products; Ashland, MA) with an average radius of 2.57 nm and a reported density of 3.65 g/cm^3. The nanoparticles are supplied in an acidic solution (pH 0.5) at a solid loading of 20 wt %. Silica suspensions are prepared by adding an appropriate amount of silica microspheres (volume fraction, ϕ_{micro}, of 0.01 or 0.10) to deionized (DI) water. The suspension is stirred for 18 h with three sonication treatments during the first 6 h. To prepare microsphere−nanoparticle mixtures, nitric acid (reagent grade; Fisher Scientific) is first added to the microsphere suspension (ϕ_{micro} of 0.10) to adjust the pH value of the suspension to 1.5 ± 0.1. Hydrous zirconia nanoparticles (volume fraction, ϕ_{nano}, of 0.00185) are subsequently added to the suspension, sonicated, and then mixed for several hours. The pH value of the mixed suspension is adjusted to 1.5, if needed, and followed by a final sonication treatment. Note that this zirconia concentration is known to stabilize the microspheres in suspension at pH 1.5 based on prior work.[11,12] In order to compare measurements of dispersed silica microsphere suspensions in the absence of nanoparticles with those obtained in the binary mixtures, a charge-stabilized microsphere suspension is prepared in DI water (pH ~ 6) to prevent the rapid aggregation that occurs between bare microspheres under more acidic conditions.

Ultrasmall-Angle X-ray Scattering Measurements. The USAXS studies are conducted at beamline 33-ID at the Advanced Photon Source, Argonne National Laboratory. This instrument employs Bonse−Hart-type[19] double-crystal optics to extend the scattering vector q range of small-angle X-ray scattering (SAXS) to a very small value, which is normally inaccessible with pinhole SAXS cameras. We used collimated and monochromatic X-rays in the standard transmission geometry[20–22] to measure the scattering intensity as a function of q. The X-ray energy is 10.3 keV, which corresponds to an X-ray wavelength of 1.20 Å.

The samples are loaded into a custom-made stainless steel cell with Kapton entrance and exit windows and a 1 mm liquid scattering path. To determine the instrumental scattering profile, two sets of USAXS measurements are collected: one with an empty cell and the other with the cell filled with solvent (DI water or pH 1.5 water). The contributions of Kapton and solvent to the scattering signal of the microsphere, nanoparticle, or microsphere−nanoparticle suspensions are eliminated in the data reduction process.

We measured the USAXS intensity over a q range from 1×10^{-4} to 0.5 Å^{-1}. The q resolution is 1.5×10^{-4} Å^{-1}. The beam size is 2.0×0.6 mm^2. The incident photon flux on the sample is 1×10^{12} photons per second, and the radiation damage is shown to be minimal.

USAXS Data Reduction and Analysis Methods. The slit-smeared USAXS data reduction and analysis are performed using the standard small-angle X-ray scattering Indra and Irena data analysis packages[23] developed at Argonne National Laboratory. The USAXS data from three samples are measured. The first sample contained only dilute monodisperse silica microspheres in DI water. The second sample contained only zirconia nanoparticles at pH 1.5. The third sample contained both monodisperse silica microspheres and hydrous zirconia nanoparticles at pH 1.5.

Both the silica microspheres and zirconia nanoparticles can be reasonably represented by a spherical morphology.[11] The scattering intensity from a spherical particle is as follows:

$$I(q) = (\Delta\rho)^2 V^2 \left[3\frac{\sin qr - qr\cos qr}{(qr)^3}\right]^2 \qquad (1)$$

where V is the volume of a sphere, r is the radius of a sphere, and $\Delta\rho$ is the difference between the scattering length densities of the solids and the solvent. The scattering contrast is $|\Delta\rho^2|$. When the scatterers are polydisperse in size, the overall intensity is a weighted sum of eq 1 and the size distribution function, so long as the probed system satisfies the dilute condition ($\phi(1 - \phi) \approx \phi$), where ϕ is the volume concentration of the scatterers.

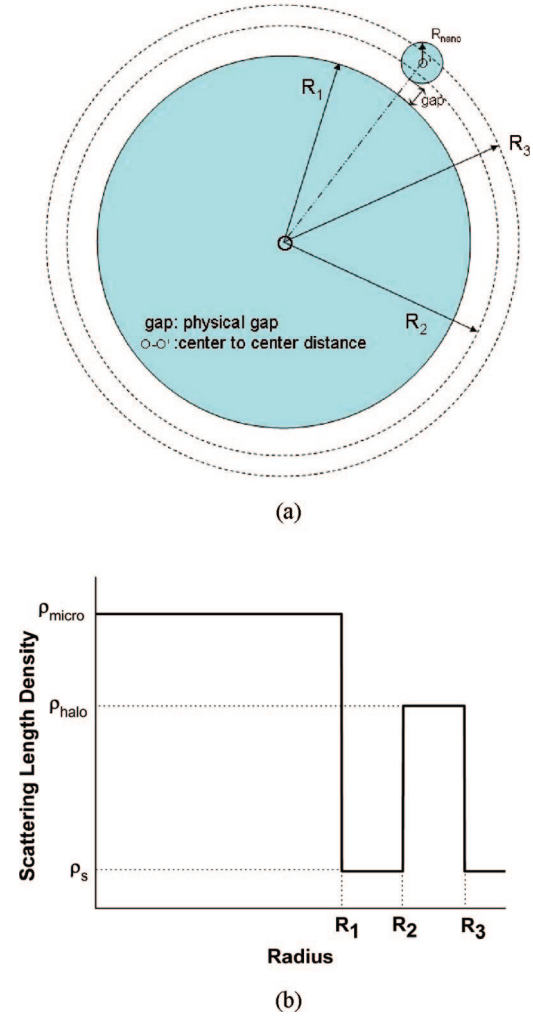

Figure 1. Schematic illustrations of (a) an individual nanoparticle near the microsphere surface (in halo) and (b) scattering length density function $\rho(r)$ used to model the nanoparticle halo, where ρ_{micro}, ρ_{halo}, and ρ_s are the scattering length densities of the silica microspheres, the nanoparticle halo, and the solvent, respectively. The microsphere radius and the effective radii of the inner and outer boundaries of the nanoparticle halo are R_1, R_2, and R_3, respectively.

To analyze the scattering profile of the binary mixtures, we assume that the electron density distribution $\rho(r)$ of the scattering objects can be described by a step function, as shown in Figure 1.

In Figure 1, the scattering length densities of the silica microsphere (core), the nanoparticle halo, and the solvent are defined as ρ_{micro}, ρ_{halo}, and ρ_s, respectively. The microsphere radius and the effective radii of the inner and outer boundaries of a shell with unknown scattering length density ρ_{halo} are R_1, R_2, and R_3, respectively. Among these parameters, ρ_{micro} and ρ_s are calculated based on the known chemical compositions and densities of the silica microspheres and the solvent. R_1 can be extracted from the analysis of the microsphere USAXS scattering profile. This leaves ρ_{halo}, R_2, and R_3 as the model-dependent fitting parameters. We note that the distances R_1 to R_2 and R_2 to R_3, which represent the modeled distance between the microspheres and nanoparticle halos and the thickness of the nanoparticle halos, respectively, are allowed by the analysis to go to zero if required by the scattering data. We allowed the distance $R_3 - R_2$ to vary because the radial scattering length density distribution of a sphere, which is not constant, differs from that of a shell, which

(19) Bonse, U.; Hart, M. *Appl. Phys. Lett.* **1965**, *7*, 238–240.
(20) Long, G. G.; Jemian, P. R.; Weertman, J. R.; Black, D. R.; Burdette, H. E.; Spal, R. *J. Appl. Crystallogr.* **1991**, *24*, 30–37.
(21) Ilavsky, J.; Jemian, P. R.; Allen, A. J.; Long, G. G. Versatile USAXS (Bonse-Hart) Facility for Advanced Materials Research. *AIP Conference Proceedings Volume 705: Synchrotron Radiation Instrumentation, Eighth International Conference on Synchrotron Radiation Instrumentation*, 2003; pp 510−513.
(22) Long, G. G.; Allen, A. J.; Ilavsky, J.; Jemian, P. R.; Zschack, P. *SRI99: Eleventh U.S. National Synchrotron Radiation Instrumentation Conference, AIP Conference Proceedings*, 2000; pp 183−187.
(23) Ilavsky, J. http://usaxs.xor.aps.anl.gov/staff/ilavsky/irena.html.

is constant. The scattering length density of a sphere is greatest at its center and decreases away from its center. Therefore, when we convert the total scattering length density of a shell populated by nanoparticles into that of a uniform shell, the effective thickness of the nanoparticle-populated shell should be smaller than the actual diameter of the nanoparticle species of which it is composed. Note that R_3-R_2 is not a physical measurement of the nanoparticle halo (or shell) thickness; however, the quantity $(R_2+R_3)/2$ does rigorously define the nanoparticle center of mass.

For a particle with a concentric scattering length density distribution, its form factor can be calculated by

$$F(q)=\int_0^\infty \rho(r)\frac{\sin(qr)}{qr}4\pi r^2\,\mathrm{d}r \qquad (2)$$

Following eq 2, the scattering form factor of a particle with the scattering length density distribution shown in Figure 1b is given by

$$F(q)=\frac{3V_1(\rho_{\mathrm{micro}}-\rho_s)J_1(qR_1)}{qR_1}+(\rho_{\mathrm{halo}}-\rho_s)\left[\frac{3V_3J_1(qR_3)}{qR_3}-\frac{3V_2J_1(qR_2)}{qR_2}\right] \qquad (3)$$

where $J_1(x)=[\sin(x)-x\cos(x)]/x^2$ is the first-order spherical Bessel function of the first kind and $V_i=(4/3)\pi R_i^3$. After being normalized to the volume of the core−shell system, the scattering intensity is

$$I(q)=\frac{A_{\mathrm{scaling}}}{V_3}\left|\frac{3V_1(\rho_{\mathrm{micro}}-\rho_s)J_1(qR_1)}{qR_1}+(\rho_{\mathrm{halo}}-\rho_s)\left[\frac{3V_3J_1(qR_3)}{qR_3}-\frac{3V_2J_1(qR_2)}{qR_2}\right]\right|^2+I_{\mathrm{bg}} \qquad (4)$$

where A_{scaling} is a scaling parameter and I_{bg} is the background intensity.

We used modeling with a least-squares fitting routine to analyze the data. For the samples containing only silica microspheres or hydrous zirconia nanoparticles, we used a one-population model assuming spherical geometry. For the microsphere−nanoparticle mixtures, we employed a two-population model to account for scattering from both the nanoparticles and the modified core−shell structure illustrated in Figure 1. In both models, we did not include multiple scattering, which was shown to be negligible.

We assumed the scattering length densities in both shells (scattering volume between $[R_1,R_2]$ and $[R_2,R_3]$) surrounding the microspheres are constant. The first shell between $[R_1,R_2]$ has the constant scattering length density of the solvent (water). The second shell between $[R_2,R_3]$ is a weighted average of the individual zirconia nanoparticles and the solvent between them.

We considered accounting for the scattering form factor with a method similar to that used in the treatment of star polymers and polymer micelles.[24,25] Because the nanoparticles are highly charged, an electrostatic repulsion prevents nanoparticle aggregation, as predicted by Rhodes and Lewis[26] using the Hogg−Healy−Fuerstenau equation.[27] Their results show a significant repulsive potential when the surface separation between two nanoparticles is about twice the nanoparticle diameter. Under these conditions, we assume that the nanoparticle−nanoparticle interference cross term can be neglected in the expression of the form factor.[24] Therefore, a modified core−shell model in eq 4 is a good approximation of the experimental system.

Results and Discussion

The scattering data obtained from the pure silica microsphere and hydrous zirconia nanoparticle suspensions are shown in Figures 2 and 3, respectively. The oscillations in the low-q region indicate that the silica microspheres have a very narrow size distribution, in good agreement with direct observations made by scanning electron microscopy (data not shown). As expected, the scattering profile of the zirconia nanoparticles appears in a relatively high-q region (in this case, 7×10^{-3} to 0.2 Å $^{-1}$) due to their smaller size.

To analyze these scattering profiles quantitatively, we calculated the X-ray scattering length density of silica microspheres, zirconia nanoparticles, and the solvent. These values are presented in Table 1. The solvent is an aqueous mixture of nitric acid (HNO_3) and deionized water (H_2O) at pH 1.5. Because nitric acid is present at low concentration (3.15×10^{-2} mol/L), it has a negligible effect on both the X-ray scattering length density and contrast of the solvent. Thus, we used the X-ray scattering length of DI water instead of that of the pH 1.5 water.

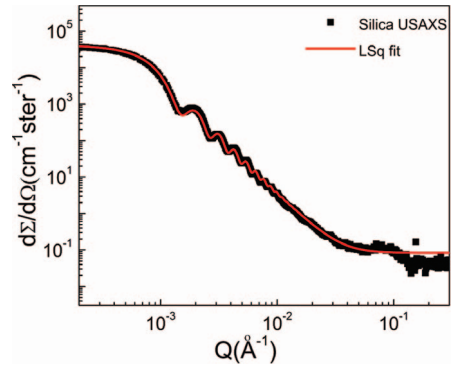

Figure 2. Slit-smeared USAXS intensity data of pure silica microspheres suspended in water and a least-squares fit.

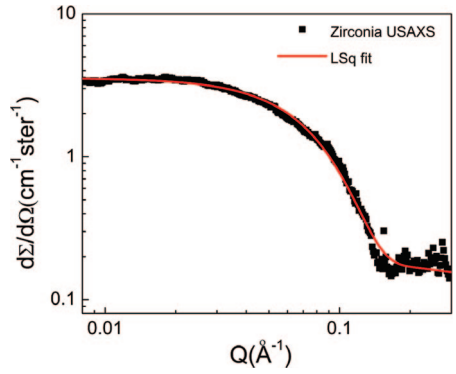

Figure 3. Slit-smeared USAXS intensity data of pure zirconia nanoparticles suspended in an aqueous solution at pH 1.5 and a least-squares fit.

Table 1. Experimental Parameters for Microsphere−Nanoparticle Mixtures

	density (g/cm^3)	X-ray scattering length density (10^{10} cm^{-2})	scattering contrast relative to solvent (10^{20} cm^{-4})
silica microspheres	2.25	18.94	91.77
zirconia nanoparticles	3.65	27.97	346.3
solvent	1.00	9.36	0

Table 2. Relative Scattering Volume, Mean Radius, and FWHM Values Determined by USAXS

	relative scattering volume	mean radius (nm)	FWHM (nm)
silica microspheres	0.34×10^{-2}	280.11	9.72
zirconia nanoparticles	0.42×10^{-2}	2.57	0.46

(24) Pedersen, J. S. *J. Chem. Phys.* **2001**, *114*, 2839–2846.
(25) Pedersen, J. S.; Gerstenberg, M. C. *Macromolecules* **1996**, *29*, 1363–1365.
(26) Rhodes, S. K.; Lewis, J. A. *J. Am. Ceram. Soc.* **2006**, *89*, 1840–1846.
(27) Hogg, R.; Healy, T. W.; Fuerstenau, D. W. *Trans. Faraday Soc.* **1966**, *62*, 1638–1651.

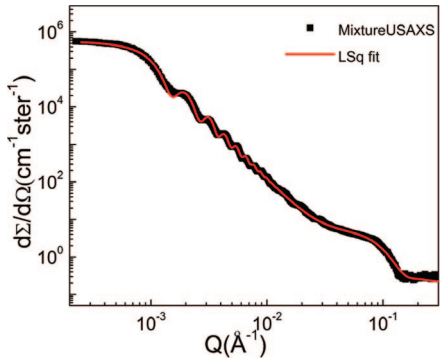

Figure 4. Slit-smeared USAXS intensity data of the silica microsphere−zirconia nanoparticle mixture suspended in an aqueous solution at pH 1.5 and a least-squares fit.

We analyzed the scattering profiles shown in Figures 2 and 3 using the form factor of eq 1, with fitted curves shown as solid lines in both figures. Because the concentration of the scatterers is low, we considered the interaction between neighboring particles to be negligible. We assumed that the size distribution of scatterers in both cases possesses a Gaussian line shape. The analyses reveal that the zirconia nanoparticles have a mean radius (R_{nano}) of 2.57 nm and the silica microspheres have a mean radius (R_{micro}) of 280.11 nm. The fitted results are listed in Table 2.

To analyze the scattering profile of the silica microsphere and zirconia nanoparticle mixture, we made the following assumptions: First, we assumed that the respective size distributions of silica microspheres and zirconia nanoparticles in the mixture are the same as those in dilute suspensions of pure microspheres and nanoparticles. Second, we assumed that the interparticle interaction between silica microspheres can be characterized by the Percus−Yevick (P−Y) pair-distribution function.[28] The P−Y pair distribution function applies to monodisperse particles with hard wall potentials. As shown in Table 2, the silica microspheres have a very narrow size distribution and can be regarded as nearly monodisperse. Also, the volume concentration of silica microspheres is reasonably low so that any interpenetration of nanoparticle halos can be neglected. Therefore, the P−Y pair distribution function provides a good approximation of the microsphere interactions.

The scattering profile of the binary mixture and its least-squares fit according to eq 4 are shown in Figure 4. The fitting parameters are provided in Table 3. In the fitting process, the minimum values for both R_2 and R_3 were set to be R_1. The USAXS-derived scattering length density of the nanoparticle-laden shell is 10.92×10^{10} cm^{-2}, which is a weighted average of the zirconia nanoparticles and the solvent within the halo. The radial scattering length density of the nanoparticles accounts for the fact that the effective thickness of the halo is less than the nanoparticle diameter. The radial scattering length density depends only on the scattering length density ρ of the sphere and the distance r from its center:

$$\rho_{radial} = \pi(R^2 - r^2)\rho \quad (5)$$

where R is the sphere radius, as shown schematically in Figure 5. The full width at half-integrated volume of the radial scattering length density $2R_{half-volume}$ is related to the spherical radius by

$$R_{half-volume}{}^3 - 3R^2R_{half-volume} + R^3 = 0 \quad (6)$$

Using eq 6, we find that $2R_{half-volume} = 0.69R$. By setting $2R_{half-volume}$ to the extracted shell thickness of 1.61 nm, we find that $R = 2.32$ nm for the nanoparticle radius, which is close to its measured radius of 2.57 nm.

(28) Percus, J. K.; Yevick, G. J. *Phys. Rev.* **1958**, *110*, 1–13.

Table 3. Fitted Radii and Scattering Length Density for Microsphere Suspensions and Microsphere−Nanoparticle Mixtures

	R_1 (nm)	R_2 (nm)	R_3 (nm)	halo scattering length density (10^{10} cm^{-2})
silica microspheres	280.11	NA	NA	NA
binary mixture	280.11	284.02	285.63	10.92

Importantly, the fitting parameters reported in Table 3 also allow us to determine whether the nanoparticles within the halo reside at some nonzero distance away from the microsphere surfaces, leading to a pure solvent layer (i.e., a gap that is devoid of nanoparticles) immediately adjacent to the microsphere surface, or if they are in direct contact. The physical gap, g, is given by $g = [1/2(R_2 + R_3) - R_{micro} - R_{nano}]$, where $R_{micro} = R_1$ and R_{nano} is 2.57 nm. Using the fitted values of R_2 and R_3, we find that there is a gap (g) of 2.15 nm between the nanoparticle and microsphere surfaces. Interestingly, the value of g is nearly equivalent to the Debye length κ^{-1} of 1.8 nm, which suggests that the nanoparticles "weakly adsorb" onto the silica microspheres with part of their counterion cloud intact.

The calibration of absolute scattering intensity is a model-free primary process with USAXS.[20] Thus we were able to determine from the scattering profile of the binary mixture that nearly 93% of the nanoparticles remain in the solution, while approximately 7% are arranged in halos around microspheres. This result suggests that the association between anoparticles and the microspheres is not strong. In addition, given that the vast majority of the nanoparticles remain in the solution, it would be very difficult, if not impossible, to discern via USAXS the internanoparticle correlation in the halo in the presence of the large uncorrelated nanoparticle population.

The USAXS data offer further opportunities to understand halo formation in these binary mixtures. We can determine the number of nanoparticles per microsphere, N_{nano}/N_{micro}, the nanoparticle volume fraction, ϕ_{halo}, and the lateral separation distance between nanoparticles, L_{halo}, within each halo, which can then be compared to values obtained from prior measurements of nanoparticle adsorption (Γ) and microsphere effective zeta potential (ζ_{eff}).[11]

The number of nanoparticles per microsphere is determined from the total scattering length of the nanoparticle shell and the average scattering length of a zirconia nanoparticle. The total scattering length, which is the integrated excess scattering length density of the shell, is attributed solely to the nanoparticles. The ratio of these two scattering lengths yields the number ratio of nanoparticles and microspheres in a halo $N_{nano}/N_{micro} = 1935$. The 2D packing "volume" fraction of the nanoparticles within

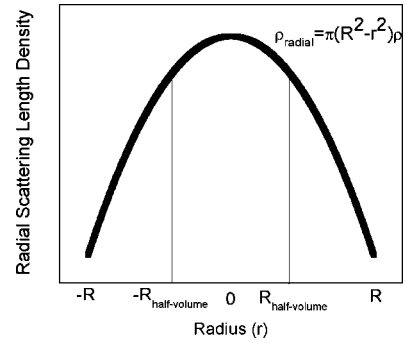

Figure 5. Schematic illustration of the radial scattering length density of a sphere as a function of distance from center, r.

Table 4. Comparison of Nanoparticle Halo Formation based on USAXS, Adsorption, and Zeta Potential Measurements

nanoparticle halo properties	USAXS	adsorption	ζ-potential
no. of nanoparticles/microsphere	1935	3280	7569
nanoparticle volume fraction	0.039	0.068	0.154
lateral separation distance (nm)	22.9	17.7	11.6

each halo is given by $\phi_{halo} \sim [N_{nano}/4N_{micro}][(R_{nano}/R_{micro})^2] = 0.039$. The lateral separation distance between nanoparticles in each halo is $L_{halo} = (\pi(R_{nano})^2/\phi_{halo})^{1/2} = 22.9$ nm (see Table 4). Although there is a substantial enrichment of nanoparticles around the microsphere surfaces compared to their volume fraction in solution, $\phi_{nano} = 0.00185$, the value of L_{halo} significantly exceeds their effective size, $2R_{nano}^{eff}$, of 9.14 nm ($\sim 2(R_{nano} + 2$ nm)), indicating that the halos remain relatively dilute.[11,12] This picture is consistent with the scattering profile of the binary mixture, which displays a high-q feature around $0.03-0.2$ Å^{-1}, indicating that a significant fraction of the nanoparticles present in suspension remains in the bulk solution. Indeed, the number ratio associated with each halo is 1 order of magnitude less than the number of nanoparticles per microsphere in solution ($\sim$25 000). These observations imply that the association between the nanoparticles and microspheres is weak, which is in good accord with both prior experimental observations[26] and Monte Carlo simulations.[14,15]

For comparison, we relate the nanoparticle surface coverage determined by adsorption measurements[11] to N_{nano}/N_{micro} by

$$\Gamma = \frac{N_{nano}}{N_{micro}} \frac{c_{nano} \times 10^{-7} \times R_{nano}^{\ 3}}{3(R_{micro} + R_{nano})^2} \qquad (7)$$

where c_{nano} is the nanoparticle concentration in g/mL, R_{micro} is the microsphere radius (equated to R_1), and R_{nano} is the nanoparticle radius. From the adsorption data (see the Supporting Information), we find that Γ is $\sim$1 mg/m^2 for the binary mixture of interest, resulting in values of $N_{nano}/N_{micro} = 3280$, $\phi_{halo} \sim (N_{nano}/4N_{micro})[(R_{nano}/R_{micro})^2] = 0.067$, and $L_{halo} = (\pi(R_{nano})^2/\phi_{halo})^{1/2} = 17.7$ nm. Collectively, these values for the number and volume fraction of nanoparticles in the halo are approximately 60% higher than those determined from the USAXS measurements (see Table 4).

For further comparison, we estimate N_{nano}/N_{micro} from the microsphere effective zeta potential, ζ_{eff}. The ζ_{eff} contains contributions from both bare and nanoparticle-associated regions on the microsphere surfaces. The measured zeta potential is related to the surface charge (Q) of a particle by the Loeb equation:[19]

$$Q = \pi\varepsilon\varepsilon_0 \frac{kT}{ze_0} \kappa\sigma^2 \left\{ 2\sinh\left(\frac{ze\zeta}{2kT}\right) + \frac{8}{\kappa\sigma} \tanh\left(\frac{ze\zeta}{4kT}\right) \right\} \qquad (8)$$

where kT is the thermal energy, z is the charge of ions in solution, e is the electron charge, $\varepsilon\varepsilon_0$ is the dielectric constant of the solution, κ^{-1} is the Debye screening length (in this case, 1.8 nm), and σ is the particle diameter. From these data, the number of associated nanoparticles per microsphere is calculated using

$$Q_{eff} = \left(\frac{N_{nano}}{N_{micro}}\right) Q_{nano} + Q_{micro} \qquad (9)$$

where Q_{nano} and Q_{micro} are the surface charges of bare nanoparticles and microspheres, respectively. Note that Q_{nano} and Q_{micro} are determined from the nanoparticle zeta potential, $\zeta_{nano} \sim 70$ mV, and the microsphere zeta potential, $\zeta_{micro} \sim 1$ mV, measured in the absence of nanoparticles. It should be noted that ζ_{nano} is estimated from the titration data reported by Peyre et al.,[29] whereas ζ_{micro} is measured directly.[11,12] From the zeta potential data (see the Supporting Information), we find that ζ_{eff} is $\sim$65 mV for the binary mixture of interest, resulting in values of $N_{nano}/N_{micro} = 7569$, $\phi_{halo} \sim [N_{nano}/4N_{micro}][(R_{nano}/R_{micro})^2] = 0.154$, and $L_{halo} = (\pi(R_{nano})^2/\phi_{halo})^{1/2} = 11.6$ nm. We note that the values for the number and volume fraction of nanoparticles in the halo are roughly 4-fold higher than those determined from the USAXS measurements (see Table 4). However, given the uncertainty in ζ_{nano} and the substantial differences between microsphere volume fraction ϕ_{micro} of 0.1 used for the USAXS and adsorption measurements relative to that of $\phi_{micro} = 0.001$ (or less) for the ζ_{eff} measurements, we have the least confidence in the latter values. Nevertheless, the entire set of data offers a striking picture. First, there is a substantive buildup of nanoparticles within a halo (or shell) near the microsphere surfaces relative to their bulk volume fraction in solution, even though the majority of the nanoparticles reside in the bulk solution. Second, the lateral spacing between nanoparticles significantly exceeds their effective size, which indicates that their effective packing fraction, $\phi_{halo}^{eff} \sim [N_{nano}/4N_{micro}][(R_{halo}^{eff}/R_{micro})^2]$, is well below that expected for strongly adsorbing species, $\phi_{ads} \sim 0.6$, which form a dense layer around each microsphere.[30] Finally, our new observations are in good agreement with both prior experiments[11,12] and theoretical predictions.[26]

Given their small size and weak attraction to the microsphere surfaces, we speculate that the nanoparticles undergo rapid diffusion both within the halo and between the bulk solution. However, neither the proposed picture outlined in Figure 1 nor the experimental technique captures the actual dynamics of the nanoparticle species. Further scattering measurements, such as X-ray photon correlation spectroscopy (XPCS), are warranted to shed light on this aspect of these novel mixtures.

Conclusion

We have investigated the distribution of nanoparticles near the surface of silica microspheres in binary mixtures stabilized by nanoparticle haloing using ultrasmall angle X-ray scattering. We have determined that the nanoparticles self-organize into a halo (or shell) that resides at a separation distance of $\sim$2 nm from the microsphere surface, which is nearly equivalent to the Debye length. We have further found that the nanoparticle concentration within this shell is significantly enriched relative to its bulk value in solution, yet the lateral separation distance between nanoparticles within each halo greatly exceeds their characteristic size. To the best of our knowledge, this is the first quantitative measurement that elucidates the spatial distribution of nanoparticles involved in the haloing effect.

Acknowledgment. Research at the Advanced Photon Source, Argonne National Laboratory is supported by the U.S. Department of Energy, Office of Science, Office of Basic Energy Sciences under Contract No. DE-AC02-06CH11357. USAXS data are collected at Beamline 33-ID. The material is based in part on work supported by the U.S. Department of Energy, Division of Materials Sciences under Award Nos. DEFG-02-91ER45439 (V.T.M. and J.A.L.) and DE-FG02-07ER46471 (J.A.L.).

Supporting Information Available: Plots of adsorption and ζ-potential data. This material is available free of charge via the Internet at http://pubs.acs.org.

LA702968N

(29) Peyre, V.; Spalla, O.; Belloni, L.; Nabavi, M. *J. Colloid Interface Sci.* **1997**, *187*, 184–200.

(30) Gilchrist, J. F.; Chan, A. T.; Weeks, E. R.; Lewis, J. A. *Langmuir* **2005**, *21*, 11040–11047.